ORNL/SPR-2023/3113

Differences in High Burnup Fuel Management Strategies to Minimize FFRD and Increase Economic Viability

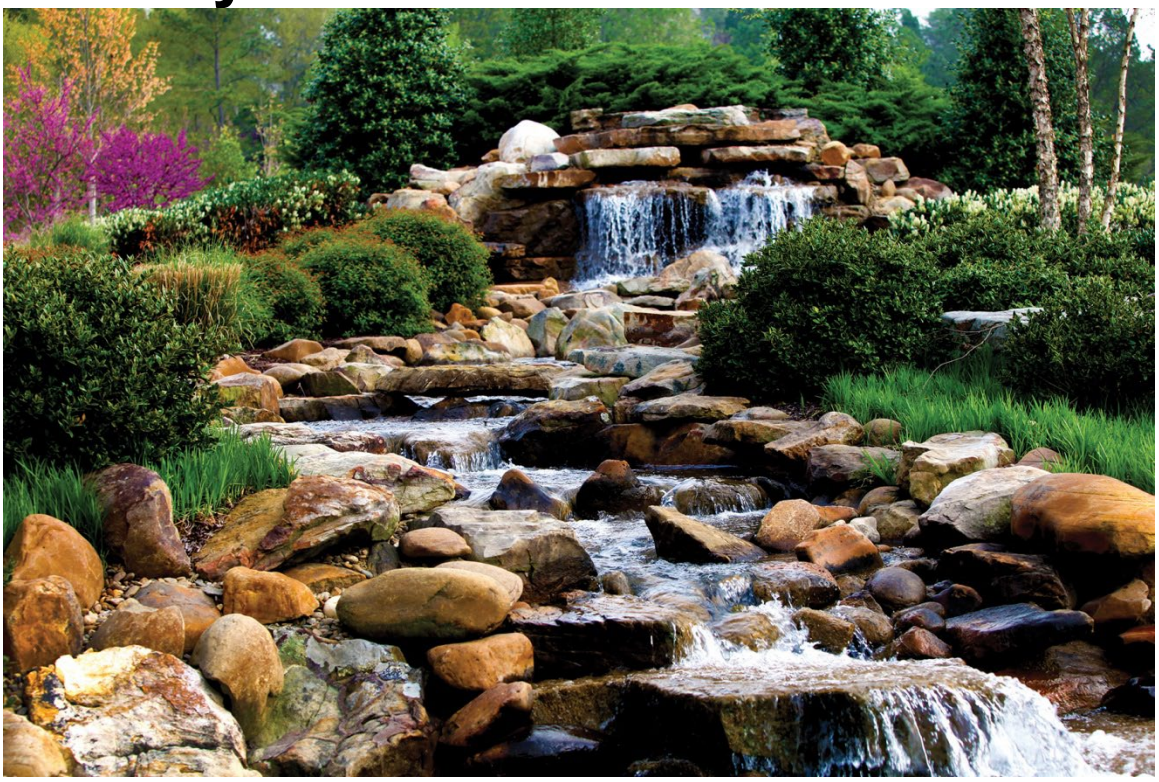

Jacob Gorton
William Gurecky
David Kropaczek
Nathan Capps

September 2023

OAK RIDGE National Laboratory

ORNL IS MANAGED BY UT-BATTELLE LLC FOR THE US DEPARTMENT OF ENERGY

ORNL/SPR-2023/3113

Nuclear Energy Advanced Modeling and Simulation

DIFFERENCES IN HIGH BURNUP FUEL MANAGEMENT STRATEGIES TO MINIMIZE FFRD AND INCREASE ECONOMIC VIABILITY

Jacob Gorton
William Gurecky
David Kropaczek
Nathan Capps

September 2023

M3MS-23OR0701051

Prepared by
OAK RIDGE NATIONAL LABORATORY
Oak Ridge, TN 37831
managed by
UT-BATTELLE LLC
for the
US DEPARTMENT OF ENERGY
under contract DE-AC05-00OR22725

CONTENTS

LIST OF FIGURES

LIST OF TABLES

ABBREVIATIONS

BU·RPF	burnup radial peaking factor
EFPD	effective full power day
EOC	end of cycle
FΔH	hot channel enthalpy rise
FFRD	fuel fragmentation, relocation, and dispersal
FGR	fission gas release
IFBA	integral fuel burnable absorber
LHR	linear heat rate
LOCA	loss-of-coolant accident
ORNL	Oak Ridge National Laboratory
PARCS	Purdue Advanced Reactor Core Simulator
PSA	parallel simulated annealing
PWR	pressurized water reactor
SNC	Southern Nuclear Company
VERA	Virtual Environment for Reactor Applications
WABA	wet annular burnable absorber

ABSTRACT

The nuclear industry is pursuing approval of an increase in the length of the pressurized water reactor (PWR) cycle from 18 months to 24 months to reduce reactor downtime and enhance the economic competitiveness of nuclear energy. Such an increase in reactor cycle length will require that the maximum rod average burnup exceeds the current regulatory limit of 62 GWd/MTU, and it could peak at approximately 75 GWd/MTU, posing potential reactor safety and performance concerns. One such concern is that fuel fragmentation, relocation, and dispersal (FFRD) could occur during a severe loss-of-coolant accident (LOCA) in which a fuel rod balloons and bursts, and pulverized fuel fragments are dispersed throughout the reactor's primary coolant system. Previous analyses have identified which reactor operating conditions leave the core more susceptible to FFRD and have shown that FFRD susceptibility is strongly linked to fuel rod burnup and linear heat rate (LHR) history. The work described in this report uses an optimization strategy known as parallel simulated annealing (PSA) and a coarse-mesh Purdue Advanced Reactor Core Simulator (PARCS) reactor physics model to develop two core fuel loading patterns, each with a different optimization objective. One core optimization maximized the core's cycle length while still respecting regulatory limits on the radial peaking factor and soluble boron concentration with a peak rod average burnup of 75 GWd/MTU. The second optimization was aimed at minimizing FFRD susceptibility while still targeting a 24-month cycle length and respecting regulatory limits. PARCS model predictions were verified using the high-fidelity Virtual Environment for Reactor Applications (VERA). The two core designs were compared to highlight core design strategies to minimize FFRD susceptibility and to maximize economic viability.

1. INTRODUCTION

The initiative to extend pressurized water reactor (PWR) cycle lengths from 18 to 24 months will require an extension to the current US Nuclear Regulatory Commission (NRC) peak rod average burnup limit of 62 GWd/MTU. This cycle length extension is motivated by the potential economic benefits of less frequent reactor shutdowns, increased reactor capacity factors, and the reduced need to purchase fresh fuel assemblies. To realize these benefits, utilities must satisfy current regulatory safety criteria surrounding accident scenarios [1]. Of primary concern is the potential for fuel to be pulverized into fine particles, coupled with a fuel rod bursting during a loss-of-coolant accident (LOCA). The combination of these events could cause fuel fragmentation, relocation, and dispersal (FFRD), in which the pulverized fuel fragments are able to escape the rod through the rupture opening and disperse throughout the reactor's primary system. Several core designs with 24-month cycle lengths have been developed following typical core design approaches and assumptions [2, 3], but the total FFRD susceptibility (measured in mass of fuel dispersed through ruptured fuel rods) has either been unassessed or was found to potentially be substantial [4]. The possibility of fuel dispersal through the reactor's primary system has long been considered by the NRC (and previously by the Atomic Energy Commission) [5], but it was repeatedly concluded that the likelihood of FFRD was too low to be considered a regulatory priority up to the current 62 GWd/MTU burnup limit. However integral and semi-integral LOCA tests performed at the Halden reactor and by Studsvik on fuel rods with pellet-averaged burnups between 55–92 GWd/MTU revealed that fuel fragments became smaller at increasing burnups and could disperse through burst openings in the cladding in the vicinity of ~67–70 GWd/MTU [1, 5]. The drive to extend reactor burnup limits to 75 GWd/MTU has reopened investigations into the FFRD phenomenon, including methods for predicting and mitigating FFRD.

This work used a parallel simulated annealing (PSA) optimization algorithm [6, 7] and reactor physics modeling tools to minimize FFRD susceptibility in a PWR while still achieving a 24-month cycle length and meeting other typical regulatory requirements. A second optimization was performed to maximize the cycle length (i.e., the economic benefit) of a PWR using equivalent regulatory constraints but with no

regard to the potential risk of FFRD. The two resulting core designs are compared to identify fuel management strategies that can minimize concerns of FFRD while still realizing the economic benefits of a 24-month cycle length.

2. METHODOLOGY

2.1 OVERVIEW

This section describes the reactor physics tools, optimization software package, and optimization constraints and objectives used for this work. The bulk of the optimizations were performed using a typical two-step reactor physics analysis method in which nuclear cross sections were generated using the Polaris module [8] of the SCALE framework [9] and then energy-collapsed for use in the Purdue Advanced Reactor Core Simulator (PARCS, v.3.4.2) diffusion code [10]. Optimized core designs were duplicated in the Virtual Environment for Reactor Applications (VERA, v. 4.3) [11] to provide high-fidelity verification of core performance and safety metrics. The optimization algorithm used for this analysis is ML-PSA [6, 12], a framework that uses a parallelized version of the constraint annealing method developed by Kropaczek and Walden [7]. RX-PSA [13], a front-end package for ML-PSA geared specifically to nuclear reactor core loading optimization, was also used. The core geometry and thermal boundary conditions remained constant throughout the analysis, and only the fuel assembly loading pattern was varied in the optimizations.

2.2 REFERENCE CORE DESCRIPTION

The geometry and thermal hydraulic boundary conditions used in the reactor model were based on a high-burnup core design developed by Southern Nuclear Company (SNC) [2] and analyzed for FFRD susceptibility during a large-break LOCA by Oak Ridge National Laboratory (ORNL) [4, 14, 15]. Parameters from the reference core that were used in this work are listed in

Table 1, and the core layout with assembly locations is shown in Figure 1. The reference equilibrium core used fuel with ^{235}U enrichments of 5.95%, 6.20%, and 6.60% with various combinations of integral fuel burnable absorber (IFBA) rods and wet annular burnable absorber (WABA) inserts. Several of the fuel assembly types developed by SNC were used in the optimizations. However, a notable feature of the SNC core design is that the peak soluble boron concentration required to maintain criticality reached nearly 1,600 ppm, which may be concerningly high because of concerns surrounding CRUD-induced power shift [16] build-up and the associated reduction of shutdown margin [17]. WABA inserts were not used in any of the fuel assembly types considered in the optimization studies. Instead, several gadolinia (Gd_2O_3) doped fuel assemblies were used to reduce the peak boron concentration while maintaining reactivity hold down. Additional details on the fuel assembly types included in the optimizations are given in Section 2.3.

Table 1. Core geometry and thermal boundary conditions from Capps et al. [2] and used in this study

Parameter	Value	Units
Core power	3,626	MW_{th}
Number of fuel assemblies	193	-
Inlet coolant temperature	291.7	°C
Coolant flow rate per assembly	85.963	kg/s
Active core height	365.76	cm
Top reflector height	36.226	cm
Bottom reflector height	16.951	cm
Fuel pellet radius	0.4096	cm
Cladding inner radius	0.418	cm
Cladding outer radius	0.475	cm
Rod pitch	1.26	cm
Assembly pitch	21.5	cm
UO_2 density	10.376	g/cm^3

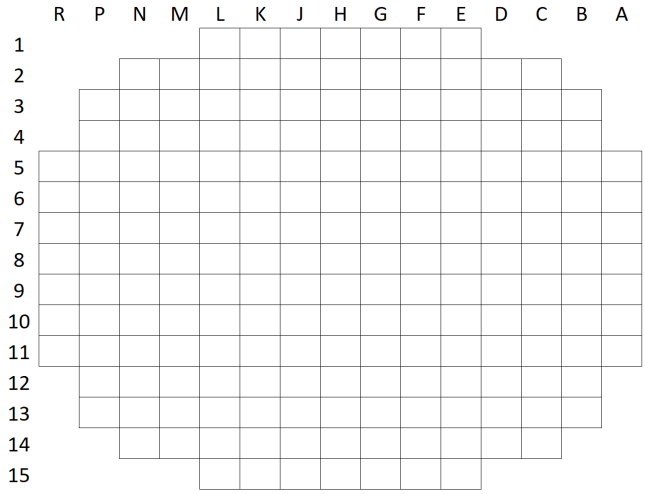

Figure 1. Reference core layout.

2.3 MODEL AND FUEL ASSEMBLY DESCRIPTIONS

The primary reactor physics modeling tools used for this work were Polaris, PARCS, and VERA. Polaris and PARCS models were adapted from those developed by Hu et al. [18] to replicate the SNC core design and fuel assemblies. VERA models were adapted from those used in previous studies at ORNL [2, 4, 14, 15]. Lattice physics calculations in 2D infinite assembly models were performed using Polaris for the 17 fuel assembly types described in Table 2. The gadolinia content (henceforth referred to simply as "Gd") in all Gd rods was 8 wt %.

Table 2. Description of fuel assemblies used in core optimizations

Fuel assembly designation	^{235}U enrichment (% ^{235}U/U)	Number of IFBA rods	Number of Gd rods
111	4.40	32	0
112	4.40	80	0
113	4.40	80	8
114	5.20	32	0
115	5.20	80	0
116	5.20	80	8
117	5.20	200	16
118	5.95	80	0
119	5.95	104	0
110	5.95	200	0
111	5.95	200	8
112	5.95	200	16
113	6.60	128	0
114	6.60	156	0
115	6.60	200	0
116	6.60	200	8
117	6.60	200	16

The Polaris depletion calculation parameters were mostly identical to those used by Hu et al. [18], with the only exceptions being in the Gd cases, which used additional radial nodes in the fuel pellet and finer burnup timesteps. All depletion calculations were carried out to 80 GWd/MTU. Figure 2 shows the various IFBA and Gd burnable absorber patterns in quarter symmetric assemblies: red pins represent regular fuel rods, yellow pins represent IFBA rods, and orange pins represent Gd rods. All lattice physics calculations were performed using a 52-group ENDF/BVII.1 cross-section library [19]. As implemented by Hu et al. [18], branch cases were simulated in Polaris for each fuel assembly type for the parameters listed in

Table 3; four values were used for each parameter. Moderator coolant temperature and density were varied simultaneously. Polaris cross-section results were energy-collapsed into the PARCS format using GenPMAXS v6.2 [20]. Cross sections for the top, bottom, and radial reflectors generated by Hu et al. [18] were directly used for this work.

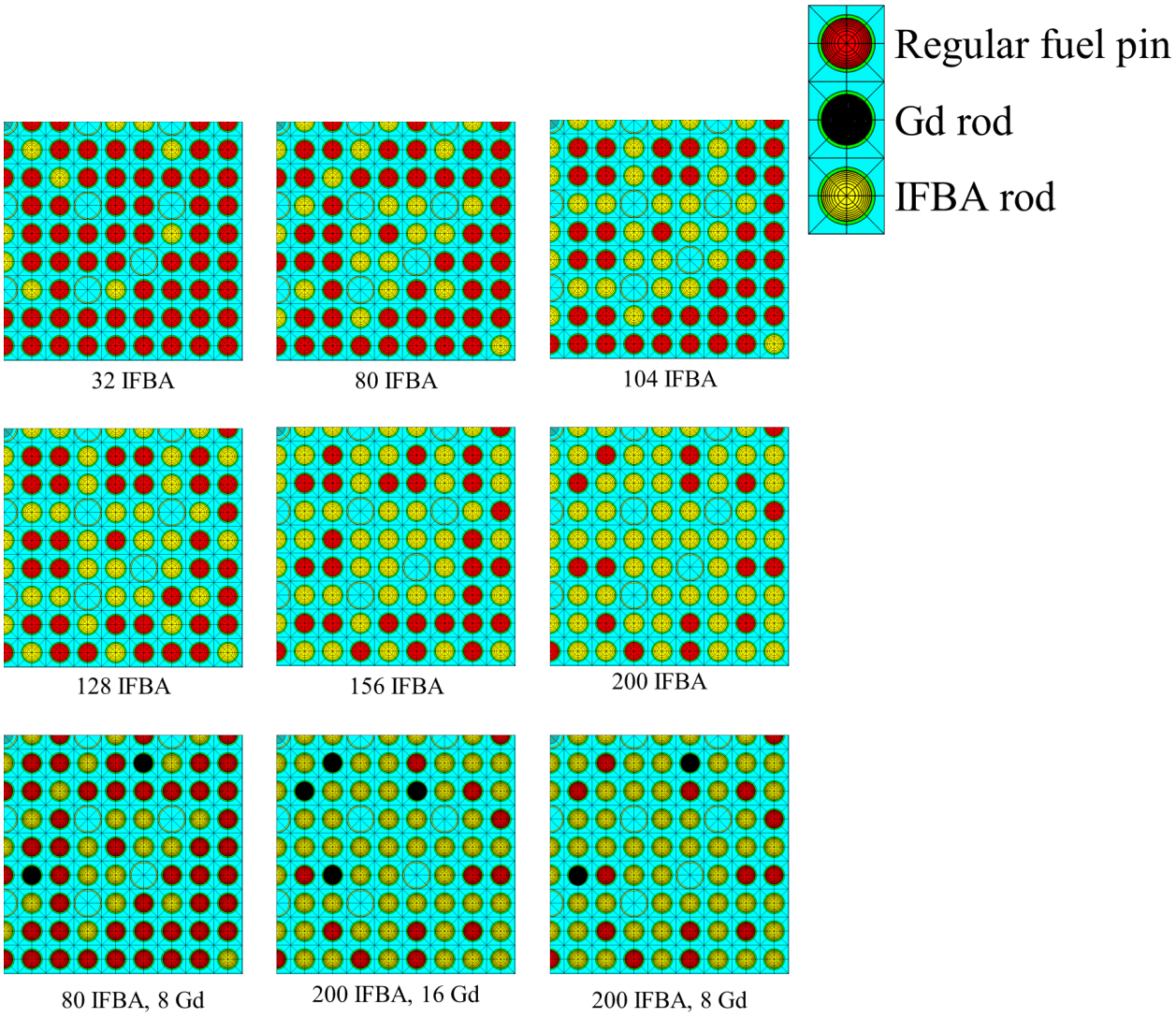

Figure 2. Quarter-symmetric depictions of each IFBA and Gd rod pattern.

Table 3. Branch parameters used for lattice physics calculations

Parameter	Value 1	Value 2	Value 3	Value 4
Moderator coolant temperature, density (K, g/cm^3)	293, 1.0052	550, 0.76971	585, 0.70045	615, 0.60811
Fuel temperature (K)	293	560	800	1,600
Soluble boron concentration (ppm)	0	600	1,800	2,500

To enhance the efficiency of the optimization studies, the PARCS models were made coarse in both the time and space domains. One axial node was used to model the bottom reflector, two axial nodes were used for the top reflector, and 12 equally sized axial nodes were used to model the active fuel region. A single radial node was used for each fuel assembly in the reactor. Grid spacers were not modeled, and the PARCS internal thermal hydraulic solver was used for thermal feedback in the cross-section lookup. In the time domain, the first depletion step was set to 10 effective full power days (EFPDs), followed by 8 steps of 45 EFPDs and then 6 steps of 60 EFPDs for a total of 730 EFPDs. The built-in equilibrium cycle capability was used so that PARCS repeated cycle calculations with a constant assembly shuffle pattern until the burnup distribution converged within a user-defined value of 0.5 GWd/MTU. The boron search method was used to find criticality at each depletion step, and the Weilandt shift method [21, 22] was enabled to accelerate convergence of the fission source iteration method. The typical PARCS runtime was approximately 2.5–6 minutes, depending on the core design and the number of cycles required to reach equilibrium. Reducing the simulation time for each core design to ≤6 minutes was crucial for exploring hundreds of thousands of core designs within a reasonable timeframe. The maximum number of cycles that PARCS was allowed to simulate without reaching equilibrium was 12. This limit was established (1) to avoid inhibitive runtimes on a single core design and (2) because cores with a constant shuffling pattern that were unable to reach equilibrium within 12 cycles likely never would.

The only changes made to the VERA models used in the previous series of works on high-burnup core designs [2, 4, 14, 15] were made to the fuel assembly definitions, assembly maps, and shuffling patterns. The fuel assembly definitions were the same as those given in Table 2, and the assembly maps and shuffling patterns were set to match the core designs resulting from the optimization studies. VERA was not used directly in the optimizations but was used to verify key figures of merit used to drive the optimization schemes. Besides the pin-resolved outputs inherently provided by VERA, the primary differences between the VERA and PARCS models were finer time and spatial nodalization, inclusion of spacer grids in the VERA models, and the use of 6-inch annular fuel blankets with no burnable poisons on the top and bottom of each fuel assembly. Fifty axial nodes were used in the active fuel region, and 40 depletion steps were used to model the 24-month cycle length. The first 10 depletion calculations were performed at 0, 0.1, 1, 3, 5, 7, 9, 11, 15, and 20 EFPDs, after which timesteps of 30 EFPDs were used.

2.4 OPTIMIZATION SCHEME

2.4.1 Parallel Simulated Annealing (PSA) Overview

Gurecky et al. [6] provide a detailed description of ML-PSA and the implementation of the constraint annealing method, a type of simulated annealing method provided by Kropaczek and Walden [7]. This section briefly reiterates the key features of ML-PSA, and Section 2.4.2 describes the specific implementation of objective functions and problem constraints to the cycle length and FFRD susceptibility optimization cases. PSA algorithms use an objective function to calculate the system's "energy" for a given set of solutions, or *system states*, to the optimization problem. New solutions are generated within the "neighborhood" of the previous system state via a Markov process dictated by a user defined, probabilistic move operator. Constraints can be applied to the optimization problem that define characteristics of a feasible solution. Critically, in the parallel constraint annealing method, each

constraint is assigned its own unique energy function and temperature. This is in contrast to typical SA implementations where the constraints and objective are scalarized into a unified single objective problem. ML-PSA solves C+1 number of concurrent, coupled optimization problems, where C is the total number of constraints imposed on the problem. This allows the constraint annealing method in ML-PSA to be penalty-free, and thus does not require choosing a scaling coefficient for each constraint. The constraint annealing algorithm allows violation of the problem constraints enroute to finding the optimal solution that satisfies all constraints because states are accepted or rejected via a local acceptance rate probability that is always nonzero. This acceptance rate probability is controlled by the objective function and constraint energies and "temperatures," which are dictated by an annealing schedule. The generic form of the local acceptance rate probability for each constraint, a_c, is given in Eq. (1):

$$a_c = \exp\left(-\frac{E_c(S^*) - E_c(S)}{T_c}\right), \tag{1}$$

where S is the current system state, S^* is the proposed system state, E_c denotes the energy function, and T_c is the current system or constraint temperature. Temperatures are set arbitrarily high during the initialization of the optimization problem (1,000, in this case), and they slowly decrease as the optimization progresses; therefore, system states that violate constraints or cause an increase in the objective function energy become less and less likely to be accepted.

The optimization problem ends when the global acceptance rate, ρ, given by Eq. (2)., falls below a certain value, which for these problems was set to 0.2:

$$\rho = \frac{\sum_p \bigwedge_{c=0}^{C}(a_c \geq u)}{P}, \tag{2}$$

where the $\wedge$ operator returns 1 if the constraint acceptance rate is greater than u, a random number uniformly selected between 0 and 1, and 0 otherwise for each chain, p, in the chain pool, P. The global acceptance rate is therefore the number of chains for which the local acceptance rate is greater than u for all constraints divided by the total number of chains being simulated in parallel. Ninety-six chains were used for both optimization problems detailed in this report. The temperatures were updated every 25 Markov steps according to the adaptive Lam and Delosme [23] cooling schedule and given in Eq. (3),

$$\frac{1}{T_{c,n+1}} = \frac{1}{T_{c,n}} + \left[\frac{\zeta}{\widehat{\sigma_c}}\right]\left[\frac{1}{T_{c,n}^{-2}\widehat{\sigma_c}^{\,2}}\right]\left[\frac{4\rho(1-\rho)^2}{(2-\rho)^2}\right], \tag{3}$$

where n indicates the cooling cycle number. The cooling cycle length was set to 25 Markov steps in this work, but this is a tune-able parameter. A cooling cycle concludes when all P parallel chains complete 25 Markov steps. ζ is a constant that defaults to 0.85 in ML-PSA, and $\widehat{\sigma_c}$ is the standard deviation of the chain energy for each constraint in the current cooling cycle. For a given cooling cycle, the computation of the temperature decrement benefits from averaging $\widehat{\sigma_c}$ over all the chains in the parallel chain pool to improve the statistics.

Finally, the parallel constraint annealing method uses a chain state mixing strategy to improve the parallel efficiency of the method and as a way promote relatively fit Markov chains, compared to other in the pool, similar to a generic algorithm. This is accomplished via a roulette style game which probabilistically eliminates low-fitness chains at end of each cooling cycle (which was set to 25 Markov steps for the computations in this report) and respawns the eliminated chains, near higher fitness chains.

At the end of each cooling cycle, a probability mass function given by Eq. 4 that defines the chain sampling probability is constructed from the energy samples generated by each Markov chain in the parallel chain pool from the last cooling cycle.

$$J_p = \frac{min_C\{F_{c=0}^p, \ \ldots, F_C^p\}}{\sum_p min_C\{F_{c=0}^p, \ \ldots, F_{c=C}^P\}} \tag{4}$$

$$F_c^p = \exp\left(-\frac{E_c^p}{T_c}\right) \tag{5}$$

Chains with poor fitness, as estimated by Eq. 5, have a low sample probability, and thus have a high chance of death. Chains with high fitness, have a higher chance of survival, and since the chains are sampled with replacement, multiple chains can be respawned in areas of the design space which contain favorable designs.

2.4.2 Problem-Specific Implementation

A custom PARCS optimization driver script was developed in RX-PSA to interface with ML-PSA for this study. Two optimizations were performed: the first focused solely on maximizing the core cycle length with no regard given to FFRD, and the second case aimed to minimize FFRD susceptibility while still achieving a 24-month cycle length. Because PARCS requires the cycle length to be defined explicitly, the objective function for the cycle length optimization case was to maximize the end-of-cycle (EOC) soluble boron concentration, whereas the cycle length was set to 730 EFPDs. A positive boron concentration at EOC indicates that the reactor could remain critical for more than 24 months, and the actual cycle length could be linearly extrapolated from the boron letdown curve.

The objective function for the FFRD case was to minimize the peak product of the instantaneous assembly radial peaking factor and the instantaneous assembly average burnup at each depletion step over the entire equilibrium cycle, henceforth referred to as the *peak assembly burnup radial peaking factor BU·RPF*. This parameter was used for the objective function based on the work of Greenquist et al. [4], who assessed the SNC high-burnup core design for FFRD susceptibility using the evaluation method devised by Capps et al. [24]. The mass of fuel susceptible to FFRD was found to be as high as ~5,400 kg [4], although this is a conservative estimate based on the combination of several worst-case scenarios and is highly dependent on the correlation used to predict cladding failure. Regardless of the assumptions and correlations used in predicting FFRD susceptibility, it is clear from that analysis that the phenomenon is strongly linked to fuel burnup and fuel rod thermal history (i.e., LHR history) [4]. These parameters influence secondary effects such as cladding embrittlement, hydrogen pickup, fission gas release (FGR), rod internal pressure, cladding strain, and the formation of high-burnup structures, all of which may increase the likelihood of cladding burst and/or fuel fragmentation. The analysis by Greenquist et al. [4] also showed that once-burned fuel rods with average burnups ≥62 GWd/MTU were the most susceptible to FFRD, likely because of the combination of high burnups and high LHRs for assemblies near the core interior. Depending on the cladding failure criteria used, between 0 and 5 out of 64 evaluated twice-burned rods were determined to be susceptible to FFRD. The low FFRD susceptibility rate in twice-burned rods was likely to the result of these rods being near the core periphery and having a low LHR, despite being the highest burnup rods in the core. These results prompted the use of the product of assembly burnup and peaking factor as the objective function for the FFRD susceptibility case.

The hot channel enthalpy rise (FΔH) factor was constrained to be ≤1.50, and the peak soluble boron concentration was constrained to ≤1,400 ppm in both optimization cases. PARCS does not report the peak rod average burnup and instead reports the peak nodal assembly average burnup. This parameter was constrained to be ≤75 GWd/MTU in both cases as a corollary to the peak rod average burnup since a

reduction in this parameter will also result in a reduction in the peak rod average burnup. VERA simulations were then used to determine the actual peak rod average burnup in the optimized cores. A limit to the number of cycles needed to reach equilibrium was set at 12; this constraint was applied to limit the computational walltime dedicated to cores that were unlikely to converge, as previously discussed. The effective multiplication factor (k_{eff}) was constrained to be ≥0.99980 in the FFRD susceptibility case to ensure that a 24-month cycle length was maintained or exceeded while allowing a small margin of error in the k_{eff} prediction in the coarse PARCS model. Finally, the problem search space was substantially reduced by using octant core symmetry. PARCS does not inherently support octant symmetry, so the RX-PSA driver script used symmetric mapping logic to sample assembly types in a core octant and then mirrored the design into quarter symmetry, which is supported in PARCS.

Although they were not used as explicit constraints, several probabilistic functions were added to the RX-PSA PARCS driver to increase the likelihood of using once- and twice-burned assemblies and to limit the number of fresh fuel assemblies to ≤95 (≤50% fresh fuel fraction) in the full core. These functions were added based on typical fuel management strategies and to enhance the economic viability of the resulting core designs. The results of an assessment by Halimi and Shirvan [3] suggest that greater fuel costs associated with higher enrichments could offset some or all the economic benefit of longer cycle lengths, and therefore greater usage of once- and twice-burned fuel will maximize the economic potential of high-burnup cores. Without these considerations, the optimizations would likely result in a core design containing fresh fuel only.

3. RESULTS

3.1 CASE 1: CYCLE LENGTH OPTIMIZATION

Figure 3 and Figure 4 show the objective function and constraint temperatures and energies, respectively, for the cycle length optimization as a function of the number of Markov steps. A temperature rapidly falling to near 0 indicates there is little variation in the constraint energy, and for the constraints given in Figure 3, means that the constraint is being met across all chains (the constraint energy is 0 across all chains). The temperature and energy plots show that the maximum boron constraint was met very early in the optimization and that the maximum burnup and FΔH constraints have both been met or nearly met. The core design produced by ML-PSA is shown in Figure 4, in which the numbers in the fresh fuel locations correspond to the assembly types in Table 2.

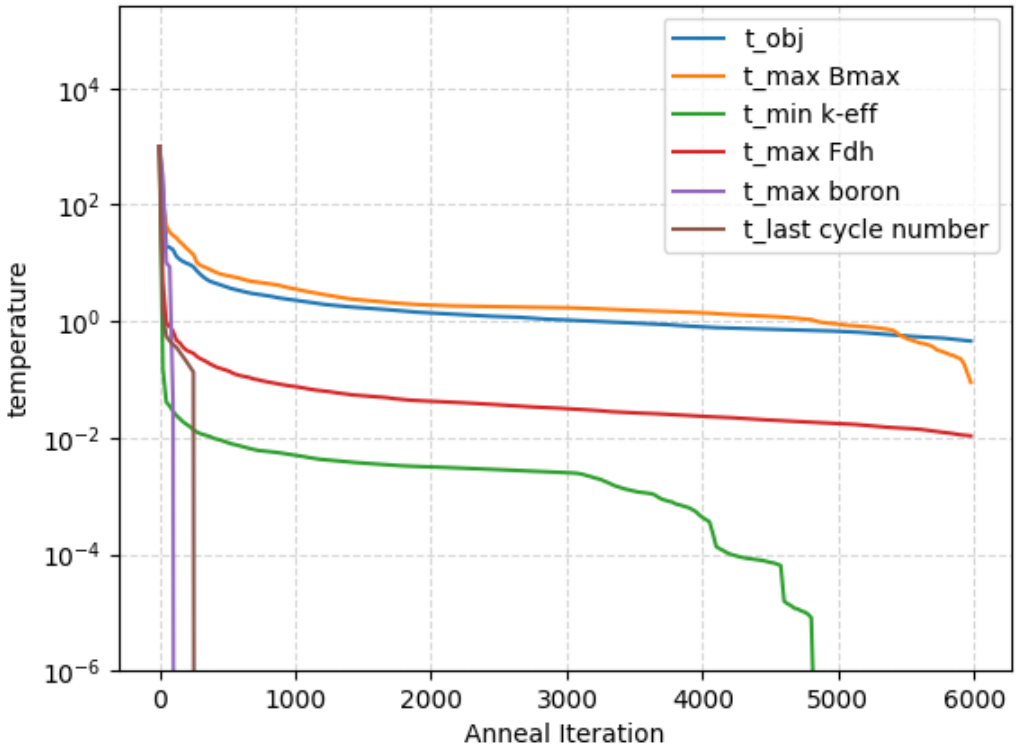

Figure 3. Objective function and constraint temperatures as a function of Markov steps.

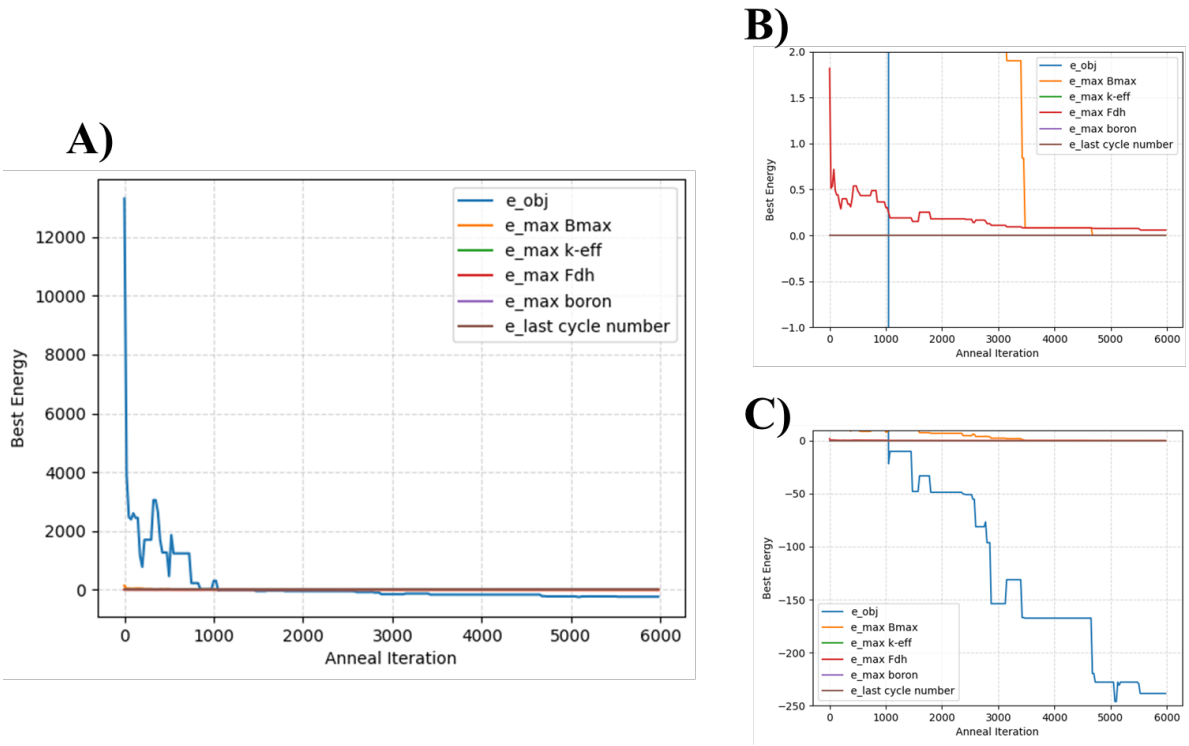

Figure 4. A shows the objective function and constraint energies as a function of Markov steps; B and C show the same information with different y-axis limits.

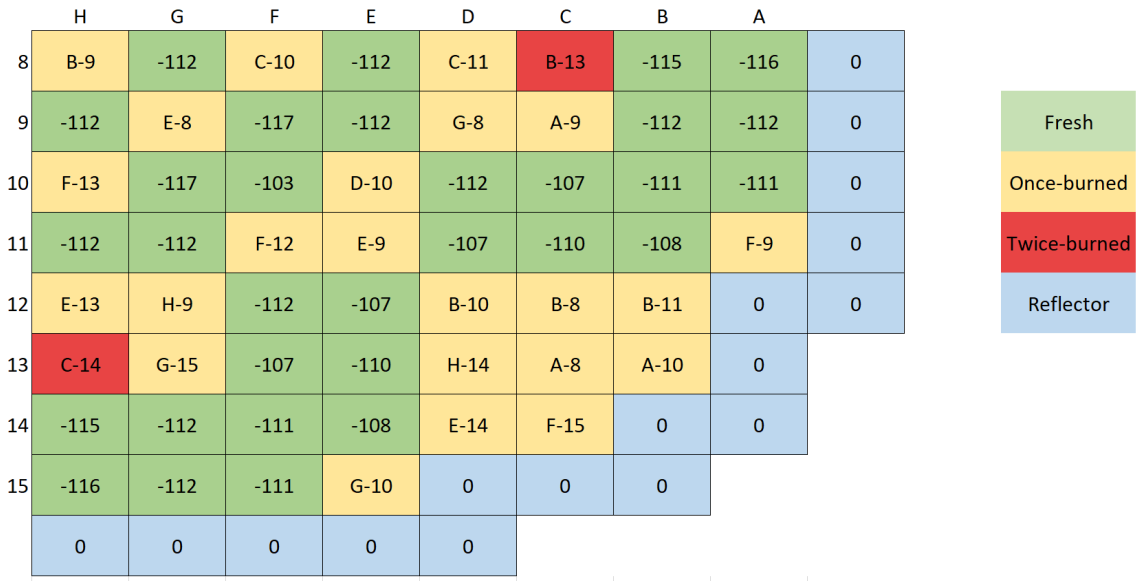

Figure 5. Quarter-core design produced by ML-PSA in the cycle length optimization.

When folded out to a full core, the core design shown in Figure 5 contains 108 fresh fuel assemblies, which would likely be considered a fraction of fresh fuel that is too high. This likely occurs because of ML-PSA move operators allowing input constraints to be violated and the algorithm preferentially selecting fresh fuel for lower burnups and longer cycle lengths. Therefore, the design was manually adjusted to achieve a fresh fuel fraction closer to 50% as shown in Figure 5. Note that the twice burned assemblies were shuffled from across the core to prevent excessive burnup gradients across those assemblies (see Figure 1 for all core locations). The adjusted core is not necessarily optimized for the constraints or objective function and was developed by making several assembly location swaps or replacements and a few enrichment adjustments to mitigate excessive peaking factors. Comparisons between the two core designs and those resulting from the FFRD susceptibility optimization are presented in Section 3.3.

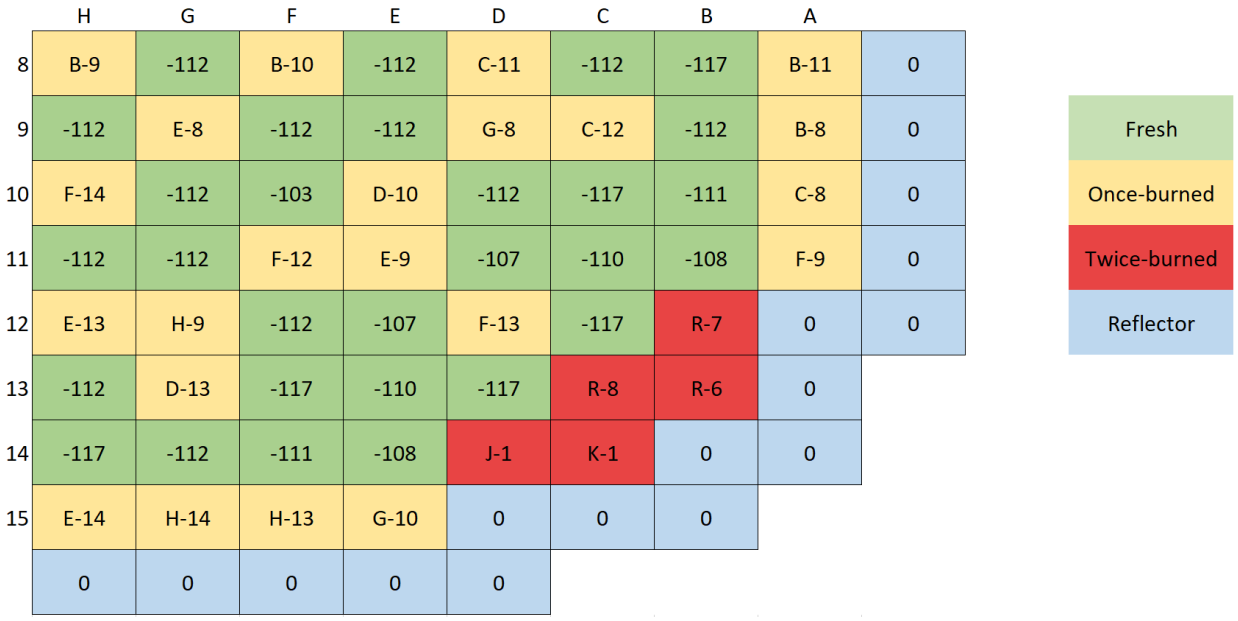

Figure 6. Adjusted core design for the cycle length optimization.

Figure 7 through Figure 9 plot the key optimization metrics (peak nodal assembly average burnup, soluble boron concentration, and FΔH, respectively) predicted by the VERA and PARCS models for both ML-PSA and adjusted core designs. PARCS results plotted after 730 EFPDs are extrapolated. The two codes were generally in agreement, with the higher fidelity code predicting somewhat higher burnups and peak FΔH values and shorter cycle lengths. The FΔH values predicted by VERA are likely higher due to rod peaking within an assembly, which is not captured in PARCS.

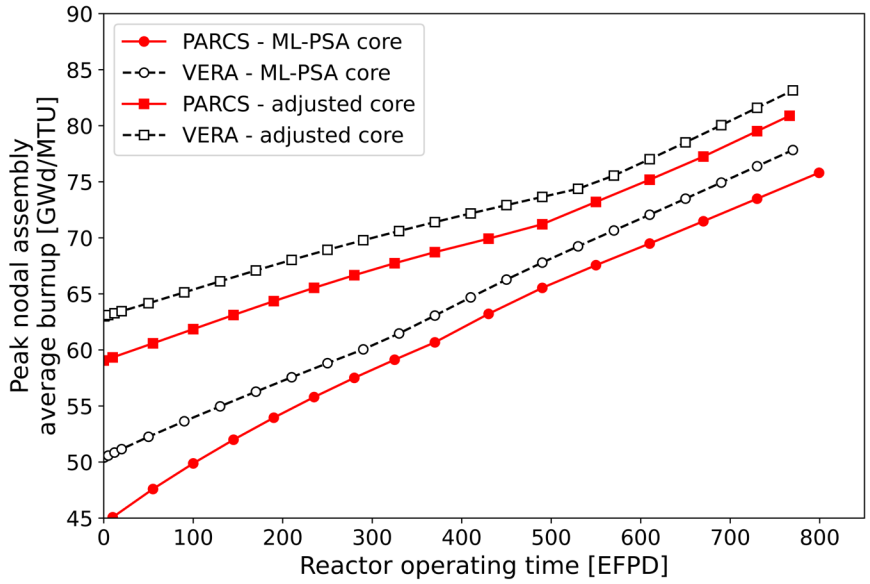

Figure 7. Comparison of VERA and PARCS peak nodal assembly average burnup predictions for the ML-PSA and adjusted core designs.

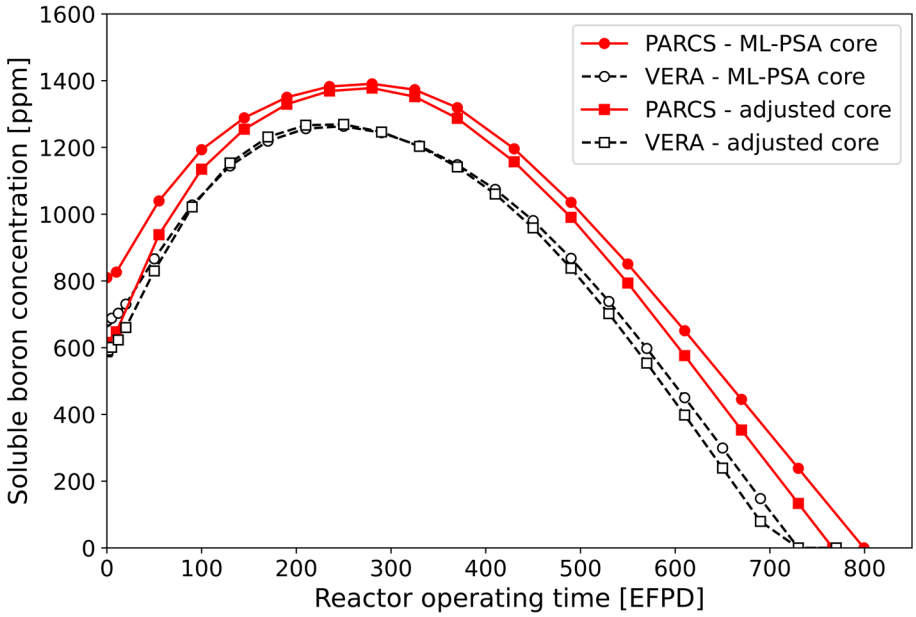

Figure 8. Comparison of VERA and PARCS soluble boron concentration predictions for the ML-PSA and adjusted core designs.

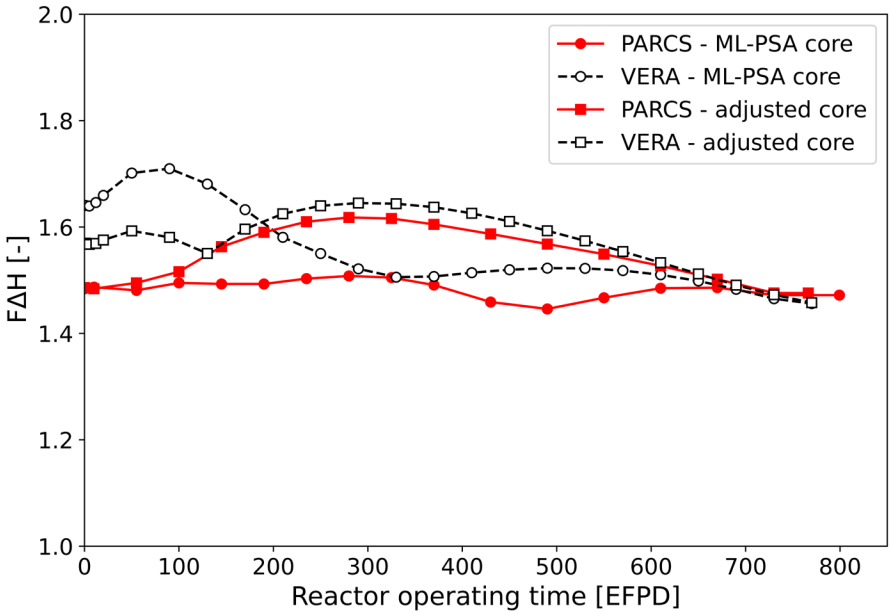

Figure 9. Comparison of VERA and PARCS FΔH predictions for the ML-PSA and adjusted core designs.

3.2 CASE 2: FFRD SUSCEPTIBILITY OPTIMIZATION

Figure 10 shows the objective and constraint temperatures as a function of Markov steps for the FFRD optimization. The results shown indicate that staying within a peak cycle boron of 1,400 ppm was easily achieved by the algorithm and that keeping the peak nodal assembly average burnup under 75 GWd/MTU was the most challenging aspect of the optimization. Figure 11 shows the energy functions for the best solution as a function of Markov steps.

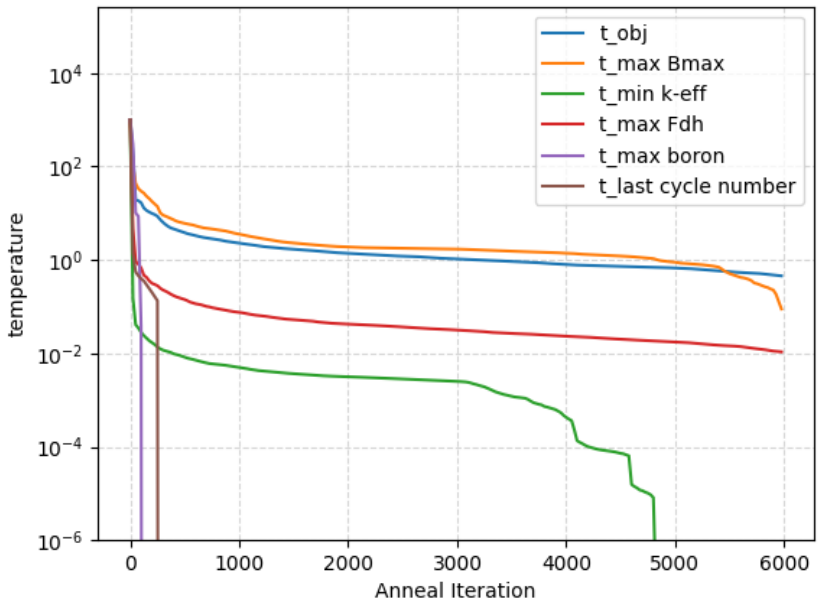

Figure 10. Objective and constraint temperatures as a function of Markov steps.

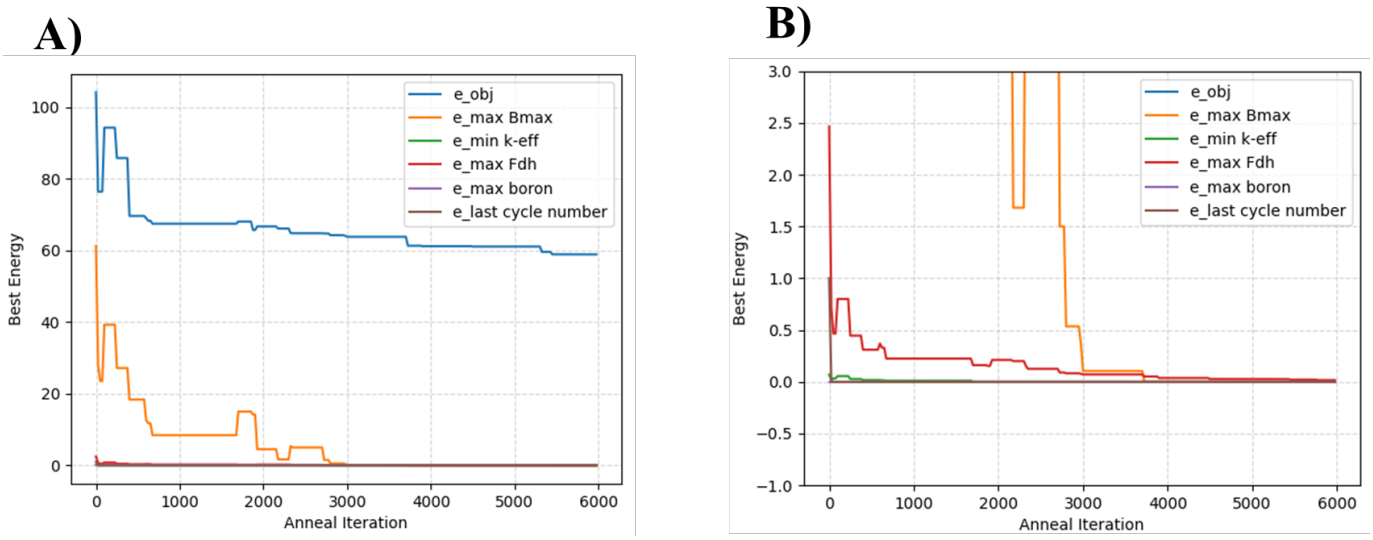

Figure 11. A: objective and constraint energies for the best solution; B: zoomed-in energy plot.

The core design produced by ML-PSA for the FFRD optimization case is shown in Figure 12. Notably, the resulting core design contains no twice-burned fuel assemblies and >50% fresh fuel fraction. The design was again manually adjusted to make the core design more feasible in terms of fuel management, and the resulting design is shown in Figure 13. Figure 14 compares the peak assembly BU·RPF between VERA and PARCS models as a function of cycle EFPDs for both the ML-PSA and adjusted core design.

	H	G	F	E	D	C	B	A	
8	-103	-107	-116	-107	B-9	-107	-107	C-12	0
9	-107	D-10	G-8	-107	E-9	A-10	-111	-114	0
10	-116	H-9	-110	-112	-112	-112	-103	-112	0
11	-107	-107	-112	C-8	B-8	-117	-114	F-8	0
12	G-14	G-11	-112	H-14	E-8	-117	A-9	0	0
13	-107	F-15	-112	-117	-117	B-11	E-10	0	
14	-107	-111	-103	-114	G-15	F-11	0	0	
15	D-13	-114	-112	H-10	0	0	0		
	0	0	0	0	0				

Fresh
Once-burned
Twice-burned
Reflector

Figure 12. Quarter-core design produced by ML-PSA in the FFRD susceptibility optimization.

	H	G	F	E	D	C	B	A	
8	-103	-112	-117	-112	B-9	-107	-117	C-12	0
9	-112	D-10	G-8	-112	E-9	B-11	-116	B-10	0
10	-117	H-9	H-8	-112	-112	-117	-112	C-10	0
11	-112	-112	-112	C-8	B-8	-117	-114	F-8	0
12	G-14	G-11	-112	H-14	E-8	-112	R-7	0	0
13	-107	E-14	-117	-117	-112	H-1	R-6	0	
14	-117	-116	-112	-114	J-1	K-1	0	0	
15	D-13	F-14	F-13	H-10	0	0	0		
	0	0	0	0	0				

Fresh
Once-burned
Twice-burned
Reflector

Figure 13. Adjusted core design for the FFRD optimization case.

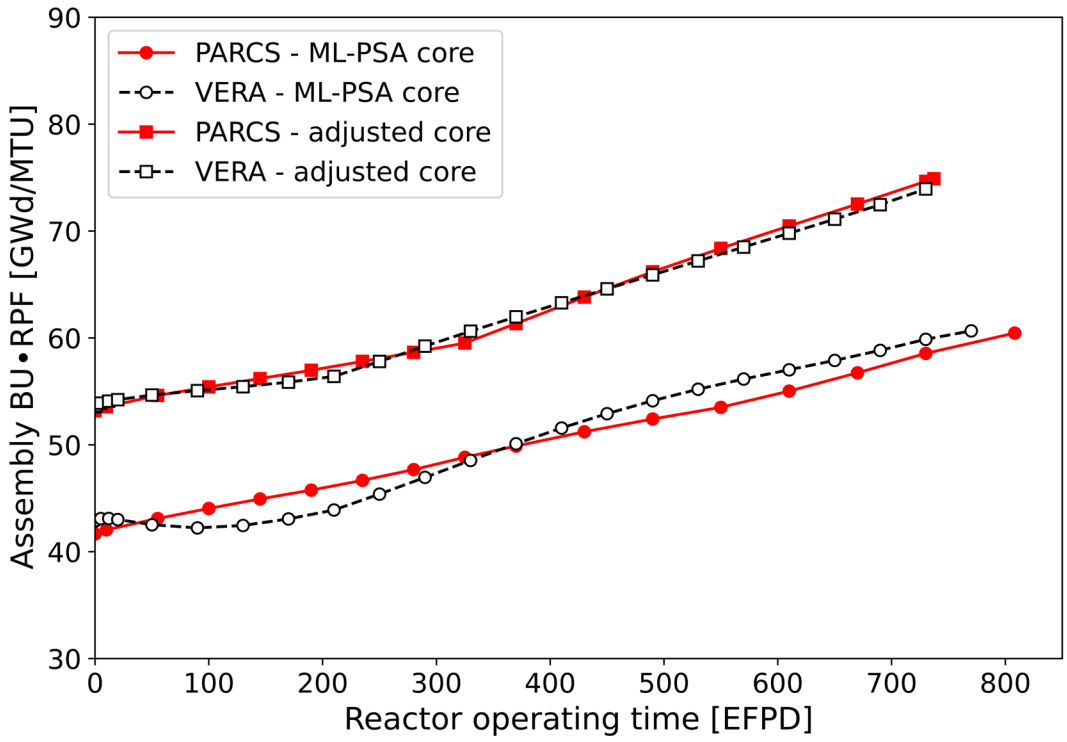

Figure 14. Comparison of VERA and PARCS BU·RPF predictions for the ML-PSA and adjusted core designs.

3.3 OPTIMIZED CORE COMPARISON

Table 4 compares the key reactor design and performance characteristics of the two cores developed by ML-PSA, the adjusted core designs, and the SNC high-burnup core design. The longest cycle length was actually achieved in the FFRD optimization case, although this design had the most fresh-fuel feeds, and the fresh fuel fraction in both ML-PSA cores was approximately 56%–58%. The adjusted cores had fresh fuel fractions in the range of 48.2%–51.8%, and the inclusion of more twice-burned assemblies and fewer fresh fuel assemblies came with a cost to the achievable cycle length. The soluble boron constraint was not violated by any of the designs, and the boron concentration was reduced by by ~300+ ppm compared to that seen using the SNC core design. This may suggest that Gd-doped rods will be critical for reactivity hold-down in high-burnup reactors. All four core designs produced in this study had longer cycle lengths than that of the SNC core design, but they required more fresh fuel assemblies, which would counteract some of the economic savings associated with a 24-month cycle. The four reactor designs also exceeded the FΔH limit of 1.5, although this constraint had been satisfied in the PARCS optimization scheme. The greater inter-assembly rod peaking could be mitigated by more optimal placement of the burnable absorber rods within the assemblies.

The peak BU·RPF was lowest in the FFRD optimization case compared with the other core designs and showed a 13.1% reduction compared to the SNC design. Further analysis with a fuel performance code would be necessary to quantify the reduction in fuel mass susceptible to FFRD associated with this reduction in BU·RPF. Tighter control over the number of fresh fuel feeds and twice-burned assemblies in the algorithm may enable further optimization of this parameter while also producing a more economically viable core. In general, the two ML-PSA cores exhibited longer cycle lengths, lower peak boron concentrations, and reduced BU·RPF, but are prohibitive in terms of fuel management and FΔH.

Table 4. Comparison of key reactor characteristics between the ML-PSA and adjusted cores as predicted by VERA. The number of fresh, once-burned, and twice-burned fuel assemblies is in a full-core

	Cycle length optimization		**FFRD susceptibility optimization**		
Parameter	**ML-PSA core**	**Adjusted core**	**ML-PSA core**	**Adjusted core**	**SNC core**
Fresh fuel assemblies	108	100	113	93	85/86
Once-burned assemblies	81	73	80	80	83/84
Twice-burned assemblies	4	20	0	20	24
Peak cycle boron concentration (ppm)	1,263	1,269	1,233	1,219	1,586
Peak rod average burnup (GWd/MTU)	74.9	81.4	73.9	77.6	75.9
Peak FΔH	1.71	1.64	1.61	1.62	1.50
Cycle length (EFPD)	729	710	743	701	693
EOC core average burnup (GWd/MTU)	47.0	50.9	46.3	49.2	51.0
Peak rod BU·RPF (GWd/MTU)	70.6	81.5	66.8	80.0	76.9

4. SUMMARY AND CONCLUSION

This work describes a PSA algorithm for optimizing PWR core designs with a 24-month cycle length with fuel burnups reaching up to 75 GWd/MTU. Two optimization studies were performed: one focused solely on maximizing the reactor cycle length to maximize the economic benefit of the core, and another focused on minimizing the core FFRD susceptibility while still achieving a 24-month cycle length. Coarse-mesh PARCS models were used in the ML-PSA optimization scheme because of short runtimes on the order of a few minutes. High-fidelity VERA models of the final core designs were used to verify the PARCS model predictions and to calculate pertinent figures of merit that could not be determined with PARCS, such as the peak rod average burnup and peak rod FΔH.

The core designs produced by the ML-PSA algorithm were able to meet or nearly meet all problem objectives and constraints but are flawed in terms of fuel management because they have too many fresh fuel feed assemblies. Both ML-PSA cores were adjusted to have more realistic fuel management schemes, which resulted in some detriment to the achievable cycle lengths, FΔH factors, peak burnups, and FFRD susceptibility. Compared to a high-burnup core previously developed by SNC, all four core designs developed in this work achieved longer cycle lengths with more reasonable soluble boron concentrations, albeit with more fresh fuel than the SNC design. A key difference from the SNC design was the use of IFBA and Gd rods in lieu of IFBA and WABA inserts, which increased reactivity hold-down and maintained the lower soluble boron concentration. Overall, this work demonstrates an approach for rapidly testing thousands of core designs to identify optimal solutions that balance reactor performance, safety, and feasibility. Future efforts will focus on implementing more robust fuel management constraints and tighter control on the number of fresh, once-burned, and twice-burned fuel assemblies, which will be critical in developing an economically feasible core design.

5. ACKNOWLEDGMENTS

This work was funded the US Department of Energy Office of Nuclear Energy (DOE-NE) Nuclear Energy Advanced Modeling and Simulation (NEAMS) program. All VERA simulations were performed using Idaho National Laboratory High Performance Computing clusters.

6. REFERENCES

[1] N. Capps, C. Jensen, F. Cappia, J. Harp, K. Terrani, N. Woolstenhulme and D. Wachs, "A critical review of high burnup fuel fragmentation, relocation, and dispersal under loss-of-coolant accident conditions," *Journal of Nuclear Materials,* p. 152750, 2021.

[2] N. Capps, A. Wysocki, A. Godfrey, B. Collins, R. Sweet, N. Brown, S. Lee, N. Szewczyk and S. Hoxie-Key, "Full core LOCA safety analysis for a PWR containing high burnup fuel," *Nuclear Engineering and Design,* vol. 379, p. 111194, 2021.

[3] A. Halimi and K. Shirvan, "Investigation of Achievable Peak Rod Average Burnup with Full Core Fuel Performance for 4-Loop PWRs," in *TopFuel 2022*, Raleigh, NC, 2022.

[4] I. Greenquist, A. Wysocki, J. Hirschhorn and N. Capps, "Multiphysics analysis of fuel fragmentation, relocation, and dispersal susceptibility-Part 1: Overview and code coupling strategies," *Annals of Nuclear Energy,* vol. 191, p. 109913, 2023.

[5] P. A. Raynaud, "Fuel Fragmentation, Relocation, and Dispersal During the Loss-of-Coolant Accident," U.S. Nuclear Regulatory Commission, NUREG-2121, 2012.

[6] W. Gurecky, B. Collins, P. Laiu, T. Pandya, Q. Huhn and D. Kropaczek, "Parallel Simulated Annealing with Embedded Machine Learning and Multifidelity Models for Reactor Core Design," in *PHYSOR 2022*, Pittsburgh, PA, 2022.

[7] D. J. Kropaczek and R. Walden, "Constraint annealing method for solution of multiconstrained nuclear fuel cycle optimization problems," *Nuclear Science and Engineering,* vol. 193, no. 5, pp. 506-522, 2019.

[8] M. A. Jessee, W. A. Wieselquist, U. Mertyurek, K. S. Kim, T. M. Evans, S. P. Hamilton and C. Gentry, "Lattice physics calculations using the embedded self-shielding method in Polaris, Part I: Methods and implementation," *Annals of Nuclear Energy,* vol. 150, p. 107830, 2021.

[9] W. A. Wieselquist and R. A. Lefebvre, "SCALE 6.3.1 User Manual," Oak Ridge National Laboratory, ORNL/TM-SCALE-6.3.1, 2023.

[10] T. Downar, A. Ward, X. Yunlin, V. Seker, N. Hudson, D. Barber, L. Larsen, B. Neykov and G. Roth, "PARCS NRC - v3.3.2 Release," University of Michigan, Ann Arbor, MI, 2020.

[11] B. Kochunas, B. Collins, S. Stimpson, R. Salko, D. Jabaay, A. Graham, Y. Liu, K. S. Kim, W. A. Wieselquist, A. Godfrey, K. Clarno, S. Palmtag, T. Downar and J. Gehin, "VERA core simulator methodology for pressurized water reactor cycle depletion," *Nuclear Science and Engineering,* vol. 185, pp. 217-231, 2017.

[12] W. Gurecky, B. Collins, D. Kropaczek, T. Pandya and M. Laiu, "ML-PSA," doi:10.11578/dc.20220110.2, 10 January 2022. [Online]. Available: https://code.ornl.gov/ml-psa/ml-psa.

[13] B. Collins, W. Gurecky, D. Kropaczek, M. Laiu and T. Pandya, "RX-PSA," doi:10.11578/dc.20221117.2, 9 August 2021. [Online].

[14] J. Hirschhorn, I. Greenquist, A. Wysocki and N. Capps, "Multiphysics analysis of fuel fragmentation, relocation, and dispersal susceptibility-PArt 2: High-burnup steady-state operating and fuel performance conditions," *Annals of Nuclear Energy,* vol. 192, p. 109952, 2023.

[15] A. Wysocki, J. Hirschhorn, I. Greenquist and N. Capps, "Multiphysics analysis of fuel fragmentation, relocation, and dispersal susceptibility-Part 3: Thermal hydraulic evaluation of large break LOCA under high-burnup conditions," *Annals of Nuclear Energy,* vol. 192, p. 109951, 2023.

[16] S. Uchida, Y. Asakura and H. Suzuki, "Deposition of boron on fuel rod surface under sub-cooled boiling conditions - An approach toward understanding AOA occurrence," *Nuclear Engineering and Design,* vol. 241, pp. 2398-2410, 2011.

[17] Electric Power Research Institute, "PWR Axial Offset Anomaly (AOA) Guidelines, Revision 1," EPRI, Palo Alto, CA, 2004.

[18] J. Hu, U. Mertyurek and W. A. Wieselquist, "Assessment of Core Physics Characteristics of Extended Enrichment and Higher Burnup LWR Fuels using the Polaris/PARCS Two-Step Approach Vol. I: PWR Fuel," Oak Ridge National Laboratory, ORNL/TM-2022/1831, 2022.

[19] M. B. Chadwick, M. Herman, P. Obložinský, M. E. Dunn, Y. Danon, A. C. Kahler, D. L. Smith, B. Pritychenko, G. Arbanas, R. Arcill, R. Brewer, D. A. Brown, R. Capote, A. D. Carlson, Y. S. Cho, H. Derrien, K. Guber, G. M. Hale, S. Hoblit, S. Holloway, T. D. Johnson, T. Kawano, B. C. Kiedrowski, H. Kim, S. Kunieda, N. M. Larson, L. Leal, J. P. Lestone, R. C. Little, E. A. McCutchan, R. E. MacFarlane, M. Maclinnes, C. M. Mattoon, R. D. McKnight, S. F. Mughabghab, G. P. Nobre, G. Palmiotti, A. Palumbo, M. T. Pigni, V. G. Pronyaev, R. O. Sayer, A. A. Sonzogni, N. C. Summers, P. Talou, I. J. Thompson, A. Trkov, R. L. Vogt, S. C. van der Marck, A. Wallner, M. C. White, D. Wiarda and P. G. Young, "ENDF/B-VII.1 nuclear daya for science and technology:

Cross sections, covariances, fission product yields and decay data," *Nuclear Data Sheets,* vol. 112, no. 12, pp. 2887-2996, 2011.

[20] Y. Xu and T. Downar, "GenPMAXS-V6, Code for Generating the PARCS Cross Section Interface File PMAXS," University of Michigan, Ann Arbor, MI, 2012.

[21] T. M. Sutton, "Wielandt iteration as applied to nodal expansion method," *Nuclear Science and Engineering,* vol. 98, pp. 169-173, 1988.

[22] B. C. Yee, B. Kochunas, E. W. Larsen and Y. Xu, "Space-dependent Wielandt shift for multigroup diffusion eigenvalue problems," *Nuclear Science and Engineering,* vol. 188, pp. 140-159, 2017.

[23] L. J. and J.-M. Delosme, "An Efficient Simulated Annealing Schedule: Implementation and Evaluation," Tech Report 8817, 1988.

[24] N. Capps, R. Sweet, B. D. Wirth, A. Nelson and K. Terrani, "Development and demonstration of a methodology to evaluate high burnup fuel susceptibility to pulverization under a loss of coolant transient," *Nuclear Engineering and Design,* vol. 366, p. 110744, 2020.